Equivalent Upscaled Hydro Mechanical Properties of a Damaged and Fractured Claystone Around a Gallery (Meuse / Haute Marne Underground Research Laboratory).

Rachid Ababou, Israel Cañamón Valera, Adrien Poutrel

Equivalent upscaled hydro-mechanical properties of a damaged and fractured claystone around a gallery (Meuse/Haute-Marne Underground Research Laboratory)

RACHID ABABOU[1]*, ISRAEL CAÑAMÓN[2] & ADRIEN POUTREL[3]

[1]*Institut de Mécanique des Fluides de Toulouse, Unité Mixte de Recherche 5502 (CNRS-INPT-UPS), 1 Allée du Professeur Camille Soula, 31400 Toulouse, France*

[2]*Departamento de Matemática Aplicada y Médodos Informáticos, Universidad Politécnica de Madrid, ETSI Minas y Energía, C./Ríos Rosas 21, 28003 Madrid, Spain*

[3]*Agence Nationale pour la Gestion des Déchets Radioactifs (ANDRA), 1/7 rue Jean Monnet, Parc de la Croix-Blanche, 92298 Châtenay-Malabry cedex, France*

**Corresponding author (e-mail: ababou@imft.fr)*

Abstract: In this work, we present calculations and analyses of equivalent continuum (upscaled) coefficients describing the damaged, fissured and fractured claystone around an underground gallery. We focus here on mechanical and coupled hydro-mechanical properties of the damaged claystone (the upscaled Darcy permeability of the same claystone was studied in a previous paper focused on hydraulics without mechanical deformations). Concerning the geometric structure of the damaged clay stone around the cylindrical excavation, we use a hybrid 3D geometric model of fissuring and fracturing, comprising (a) a set of 10 000 statistical fissures with radially inhomogeneous statistics (size, thickness and density increasing near the wall), and (b) a deterministic set of large curved 'chevrons' fractures, periodically spaced along the axis of the drift according to a 3D chevron pattern. The hydro-mechanical coefficients calculated here are second- and fourth-rank tensors, which are displayed using ellipsoids. For simplicity, we also calculate equivalent isotropic coefficients extracted from these tensors: Young's modulus (E), bulk modulus (K), Lamé shear modulus (μ), Poisson's ratio (ν), Biot coefficient (B, stress–pressure coupling) and Biot modulus (M, pressure–fluid production coupling). All of these coefficients are affected by the degree of damage and fracturing, which increases near the wall of the gallery. Both 3D and '2D transverse' distributions are analysed, on grids of 3D cubic voxels and 2D pixels, respectively. Global coefficients upscaled over the entire damaged and fractured zone are also analysed. Other types of averages are presented, for example, upscaled values over a cylindrical annular shell at various radial distances from the gallery wall. The relation to the degree of fracturing is discussed, including for instance the effect of fracturing on bulk and shear stiffnesses, and on the hydro-mechanical coupling coefficients of the damaged claystone.

The main objective in this paper is to determine by *homogenization*, or *upscaling* from fine to coarser scales, the coupled hydro-mechanical (H-M) behaviour of a damaged (fissured and fractured), water-saturated porous clay rock around a cylindrical excavation. Here, the term 'upscaling' is used in the following sense: obtaining equivalent continuum properties for the fractured porous rock at selected scales (averaging volumes). The excavation considered in this work is a subhorizontal cylindrical 'drift' (named the GMR gallery), located at about 525 m depth in the Underground Research Laboratory (URL) 'CMHM' (Centre de Meuse/Haute-Marne, Bure, France) operated by ANDRA. This URL is used to develop research studies on the stability and isolation properties of a deep geological repository for radioactive waste in Callovo-Oxfordian claystone.

In this context, a programme was developed towards the simulation of hydraulic, mechanical and coupled hydro-mechanical processes in the near field, in the damaged and fractured zone around a cylindrical underground excavation. Our objective is to obtain a set of 'upscaled' continuum equivalent equations and coefficients, based on the geometry and properties of the discrete fractures, and based on the properties of the porous rock matrix. The zone of interest is the so-called excavation damaged zone (EDZ), a cylindrical annular zone around the gallery. The next section will present the study site briefly, but we also refer the interested reader to Ababou *et al.* (2011) for more

details concerning the overall objectives, the programmatic context, the URL site and some of the relevant data.

To sum up, the present work focuses on obtaining a continuum equivalent model (and the corresponding 'upscaled' coefficients) for coupled hydro-mechanical processes in the EDZ around a cylindrical excavation (gallery).

Specifically, we are interested in achieving this continuum characterization in three dimensions (3D) by a fast method that does not require detailed numerical equations for the processes taking place in the fractured porous rock to be solved. On the other hand, we require that the method is able to take into account in some way the 3D geometric structure and the hydro-mechanical properties of the fractures (embedded discontinuities) and of the 'intact' porous rock (embedding matrix).

The present paper elaborates on a previous presentation by the authors at the Clay 2012 conference (Ababou *et al*. 2012).

Basis of the superposition method for upscaling

With this in mind, we have selected a computationally fast upscaling method that can be considered as a *generalized superposition method*. Superposition methods have been used for upscaling permeability in fractured media (quite frequently), and also sometimes (more rarely) for upscaling hydro-mechanical processes in fractured media, but without including the full role of the water-filled matrix porosity in these processes. Thus, in Oda (1986) and Stietel *et al.* (1996), the rock matrix is impervious hydraulically, and does not participate in pressure–stress coupling mechanically. Similarly, the recent paper by Sævik *et al.* (2013) includes a section on superposition methods, where the fractured medium is assumed to be made up of fractures imbedded in a totally impervious matrix.

Note: in addition to the superposition methods (effective medium approximation), there are several other groups of upscaling methods, such as the Self-Consistent approximations and their variants (e.g. Sævik *et al.* 2013), and there are many other upscaling methods, some quasi-analytical and some others numerical, which are all largely developed in the literature. Even if we do not aim to discuss these other methods in this paper, we briefly discuss their main limitations to state the benefits of the superposition method in the case of fractured porous media. For example, the Self-Consistent approximation has well-known limitations for high density of fracturing (while the superposition approach, on the contrary, performs well for high-density fracturing but has drawbacks for low-density or poorly connected systems). There are also methods that are more heavily numerical, where the upscaled coefficients are computed by solving a detailed solution of partial differential equations (PDEs) that are similar in complexity to the non-homogenized PDEs themselves. Such methods are therefore more computationally intensive, and expensive, than the superposition approach. Finally, there are also numerical solvers that aim at obtaining detailed simulations of the behaviour of the porous matrix, the discrete fractures and their interactions. In some cases, these solvers use a set of local-scale effective coefficients, such as the parallel and orthogonal effective permeability of a joint embedded in a porous matrix (this concept was also used in Cañamón (2006, 2009) and Ababou *et al.* (2011) as a building block for implementing the hydraulic superposition method on larger scales). For instance, Mourzenko *et al.* (2010) numerically solve single-phase flow in a matrix–fracture system with thousands of fractures, tens of wells and millions of elementary volumes, with local effective permeability attributed locally to the discrete joints surrounded by porous matrix.

In the present paper, on the other hand, the aim is to upscale, not to simulate, and the method for upscaling is to extend the superposition approach to obtain a fast evaluation of global and spatially distributed upscaled coefficients describing the coupled H-M properties of the fractured porous rock on chosen support scales. In this upscaled description, the rock is viewed as an equivalent H-M continuum. The resulting coefficients can potentially be used as inputs for numerical simulations using more or less 'standard' H-M solvers and codes accepting tensorial coefficients, and this without the need for a detailed representation of fractures. In this paper, we calculate and analyse the upscaled coefficients without implementing the simulations themselves.

The *generalized* superposition method considered in this paper goes as follows:

- For hydraulic upscaling, the local Darcy and/or Poiseuille fluxes in both the permeable matrix and the cracks are superposed, and the final result is a tensorial flux/gradient law with macro-permeability K_{ij} (this problem is fully treated in Ababou *et al.* (2011) for the same URL site and the same GMR gallery).
- For mechanical upscaling, local strains are superposed, in a manner that involves both the isotropic elastic porous matrix and the strongly anisotropic elastic cracks. When the coupling is ignored, this results in continuum equivalent

tensorial coefficients of compliance (C_{ijkl}) and stiffness (R_{ijkl}).
- When taking into account fully coupled H-M processes (the object of this paper), the local strains in the matrix and cracks are still being superposed but, in addition, the interactions with variations of fluid pressure and with fluid production are also taken into account. Moreover, these interactions occur both in the water-filled cracks and in the saturated porous matrix. At least two new coefficients are thus obtained, the Biot coefficient, B_{ij}, and the Biot modulus, M (described in more detail below).

Our implementation of the effective medium/superposition method, to date, does not deal explicitly with fracture–fracture interactions. On the other hand, by various refinements of the method, we account here for the following types of interactions in 3D: (a) pressure–stress coupling and fluid production within the matrix; (b) pressure–stress coupling and fluid production within the fracture system; and (c) hydro-mechanical matrix–fracture interactions.

The tensorial superposition calculations leading to C_{ijkl}, R_{ijkl}, B_{ij} and M, are rather involved. Some relevant theoretical relations thus obtained will be presented in this paper, along with the quantitative results obtained specifically for the EDZ around the gallery of our study site.

In practice, for our specific application, the upscaling method is implemented as follows:

- Implementation starts with the definition of a permeable and deformable porous rock matrix, and with the specification of several sets of discrete embedded cracks or fractures. In the present case, we have two main sets: (a) a statistical set of small planar disc fissures (joints, cracks); and (b) a deterministic set of large curved fractures organized in a periodic 'chevron' pattern. The latter fractures are then numerically discretized into triangular patches before applying the generalized superposition method (see Ababou *et al.* 2011). The statistical cracks are disc-shaped planar objects that are generated only once (single realization). In the end, all planar 'fractures' or 'cracks' resulting from these procedures are stored in a unique object database, with 3D geometric parameters and other properties attributed to each crack. It should be emphasized that the cracks are hydro-mechanical as well as geometric objects: they are hydraulic conductors, and they are deformable objects. In particular, they all contribute to pressure–stress coupling, as does the porous rock matrix itself (further details on this are given below).
- Finally, given the geometric, hydraulic and mechanical properties of these materials at the local scale (the intact claystone matrix and the various types of cracks), the superposition method yields an upscaled system of continuum laws (Darcy, Hooke, Biot) with equivalent continuum coefficients (tensors), such as mechanical stiffnesses and H-M coupling coefficients, as mentioned earlier.

Concerning the equivalent Darcy law, and the calculation of macropermeability, we recall again that this was addressed separately in a previous work (Ababou *et al.* 2011). The macroscale permeability tensor K_{ij} was calculated in the EDZ using the flux superposition method. Therefore, in this work, we need only be concerned with the upscaling of coupled H-M properties, using the generalized strain superposition method sketched earlier.

Finally, let us discuss the 'scale' at which the equivalent continuum is calculated. In our procedure, the 'equivalent continuum' coefficients are evaluated at some specified 'homogenization scale' (meso- or macroscale), which is analogous to the support scale or measurement scale of a field measurement (its volume of influence). We will see in this paper how the upscaled coefficients obtained in the EDZ depend on the chosen scale of homogenization. When the selected scale is sufficiently 'local' (e.g. with respect to gallery diameter), we obtain not only the numerical values but also the spatial distributions of these upscaled coefficients within the damaged zone around the gallery (EDZ).

Several types of spatial distributions will be analysed, depending on the selected scales and supports of averaging:

- 3D spatial distributions obtained by upscaling locally on small cubic voxels (0.5 m);
- 2D transverse distributions of H-M properties – these are obtained by upscaling along the entire axis of the gallery as well as transversely on a grid square pixels (0.5 m);
- 1D radial distributions – these are obtained by upscaling on annular regions, that is, over cylindrical annular shells (thickness 0.5 m) located at various radial distances from the drift wall;
- 0D global coefficients ate the scale of the entire EDZ – these are obtained by upscaling over the entire damaged and fractured zone around the cylindrical drift (here the drift radius is 2 m and the total thickness of global annular shell is taken to be 4.0 m).

We expect that these types of results, taken together, will lead to a simplified quantification of the effects of fracturing on the claystone stiffness, and on the

Hydro-Mechanical coupling coefficients, at various scales of analyses.

Application site (Underground Research Laboratory)

The parameters used in the upscaling calculations presented later on in this paper correspond to the CMHM (Centre de Meuse/Haute-Marne, Bure, France), the Underground Research Laboratory (URL) operated by ANDRA – the French national agency for the management of radioactive waste.

We focus here on the damaged zone around the 'GMR' gallery, a subhorizontal gallery, located at about 525 m depth underground, within the Callovo-Oxfordian formation, a thick 130 m claystone layer between depths 400 and 600 m. The GMR gallery is oriented parallel to the minor horizontal principal stress (σ_h). For more details, we refer the interested reader to Ababou *et al.* (2011) and references therein, concerning the overall scientific objectives, the programmatic context, the URL site and some of the available *in-situ* data and observations.

For instance, see Armand & ANDRA (2007) concerning measurements of radial permeability profiles, and observations of rock fracture traces in the EDZ around galleries at the URL site (including the GMR gallery and other galleries).

The reader may consult other publications (Vincké *et al.* 1997; Coste *et al.* 1999; Cosenza *et al.* 2002) concerning various evaluations of mechanical and hydro-mechanical coefficients in the Callovo-Oxfordian claystone. We will refer more precisely to these works when discussing results (see section on 'Inputs, results, analyses: equivalent H-M coefficients').

Finally, the reader may consult ANDRA (2005*b*) for an overall description of ANDRA's URL site and its objectives.

Based on *in-situ* observations like those of Armand & ANDRA (2007) and others, it was decided that the geometric structure of fissures and fractures around the gallery should be represented by combining two sets: a statistical set of planar disc cracks, and a deterministic set of large curved chevron fracture surfaces (as explained in the previous section on objectives and methods). In summary, the small disc fractures (which contribute essentially to near-wall damage) are represented statistically, while the large curved fractures (which have a larger extent that the diameter of the drift) are modelled as deterministic parametric surfaces, periodically arranged along the drift axis. These two synthetic sets of fractures constitute essentially our 'model' for the internal geometric structure of the fractured and damaged EDZ. This is defined more quantitatively in the next section.

Geometric structure of fissured and fractured claystone

Concerning the geometric structure of the damaged claystone around the cylindrical excavation (gallery), we use a hybrid statistical and deterministic geometric model of 3D fissuring and fracturing, comprising:

(1) A statistical set of 10 000 randomly distributed and randomly oriented, disc-shaped planar fissures. This set has radially inhomogeneous statistics: in particular, the fractures are more densely distributed near the wall. Some of the statistical/geometric parameters of this random set of cracks were calibrated by comparing upscaled permeabilities with measured permeability profiles along radial boreholes (Ababou *et al.* 2011).

(2) A deterministic set of large curved 'chevron' fractures, periodically distributed along the axis of the gallery (inter-spacing 0.5 m) and forming a 3D chevron pattern. The curved surface of each large 'chevron' fracture was represented using a parametric surface model (a modified *conoidal* surface resembling the pinched end of a toothpaste tube). These curved fractures surfaces were further discretized into triangular planar cracks (patches).

The complete 3D system of fractures is shown in Figure 1.

The reader is referred to Ababou *et al.* (2011) for more details on the procedures that allowed us to generate and represent each subset of fractures, and for a description of the complete set of geometric parameters, statistical as well as deterministic.

Theory and equations of the upscaling method

Equivalent continuum equations, tensorial coefficients and variables

The upscaled behaviour of the claystone is described by a system of coupled equivalent continuum hydro-mechanical PDEs that enforce mass conservation and (quasi-static) momentum conservation. The variables involved are total stress (σ_{ij} or $\Delta\sigma_{ij}$), total strain (ε_{ij}), and water pressure (p or Δp). Other variables involved are the water flux density vector (q_i) expressed by Darcy's law (Darcy 1856), and the water production term $\Delta\xi$

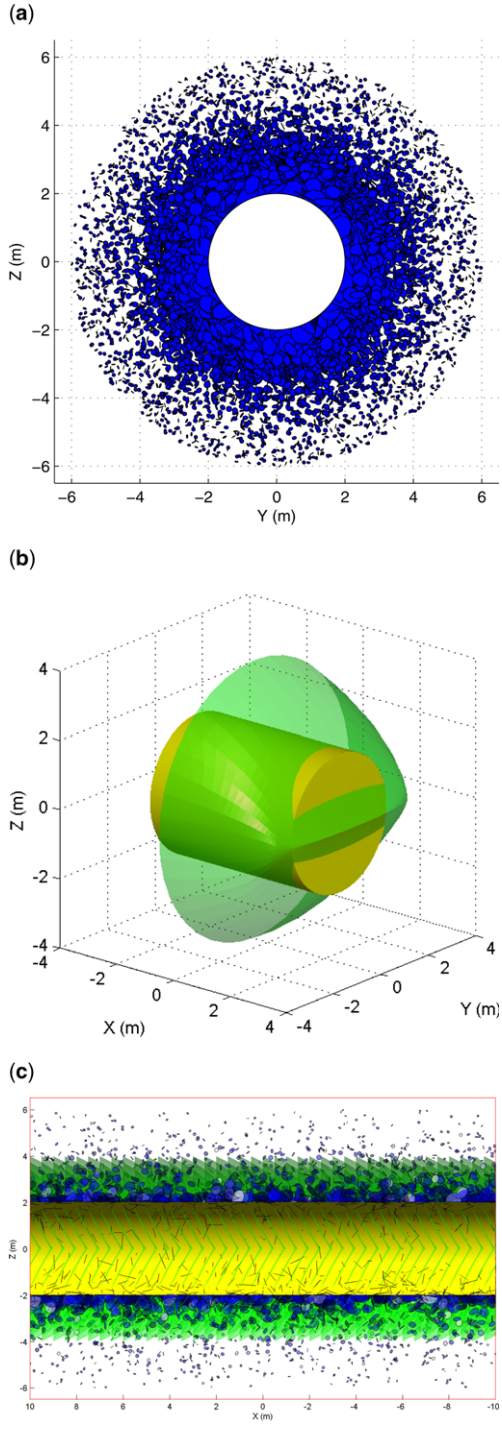

Fig. 1. (**a**) 2D transverse view of the statistical set of fissures (small fractures); (**b**) 3D view of a single curved chevron fracture surface; (**c**) 2D longitudinal section of the fissured and fractured system.

(defined further below). All these variables depend on 3D space and time. The symbol Δ designates a variation in time at any given point (x, y, z).

The mesoscale equivalent continuum equations obtained by our generalized superposition method take the form of linear *tensorial laws involving tensorial coefficients*, all the coefficients being calculated in terms of the given geometric structure and properties of the fractures and of the porous rock matrix (*note: we use everywhere Einstein's notation of implicit sum on repeated indices, unless mentioned otherwise*).

- Hooke's stress–strain law (without H-M coupling) contains tensorial stiffness coefficients R_{ijkl} (Pa),

$$\Delta\sigma_{ij} = R^{\mathrm{MC}}_{ijkl}\,\varepsilon_{kl} \tag{1}$$

  where the superscript MC denotes 'matrix and cracks' (i.e. the equivalent homogenized medium). Some classical scalar coefficients can be derived by various contractions of the upscaled R_{ijkl} tensor, a process we call '*isotropization*' (a neologism described in Appendix 1). In this way, we obtain, for instance, isotropic equivalent values of Young's modulus E, the bulk modulus K, the shear modulus μ and Poisson's ratio ν. This will be useful when calculating the equivalent tensor R_{ijkl} on annular regions or at the global scale of the entire EDZ; however, the full anisotropic R_{ijkl} tensor is of more interest on local scales (i.e. half-metre-scale cubic voxels).
- The hydro-mechanical Hooke/Biot stress–strain–pressure law contains a pressure term that couples stress to pressure via a tensorial Biot coefficient B_{ij} as follows:

$$\sigma_{ij} = R^{\mathrm{MC}}_{ijkl}\,\Delta\varepsilon_{kl} + B^{\mathrm{MC}}_{ij}\,\Delta p \tag{2a}$$

$$\varepsilon_{ij} = C^{\mathrm{MC}}_{ijkl}\,\Delta\sigma_{kl} + \bar{B}^{\mathrm{MC}}_{ij}\,\Delta p \tag{2b}$$

In equation (2a), σ_{ij} is the stress tensor, R_{ijkl} is the stiffness tensor, ε_{ij} is the strain tensor, B_{ij} is a dimensionless 'Biot' coupling coefficient and p is the water pressure. All stresses are taken as negative under compression (thus, fluid stress is $-p\delta_{ij}$). Note that Terzaghi's (1936) 'effective stress' model corresponds to $B_{ij} = 1 \times \delta_{ij}$ (effective stress $\sigma_{ij} + p\delta_{ij}$). Biot's (1941, 1956) theory generalizes Terzaghi by considering a scalar coupling coefficient B such that $0 < B \leq 1$ (effective stress $\sigma_{ij} + B\,p\delta_{ij}$). In the more general model here, B_{ij} is a tensorial coupling coefficient obtained by upscaling the saturated porous rock with its water-filled cracks. The tensor $\bar{B}_{ij}$ appearing in equation (2b) is called

in this work the 'reciprocal Biot coefficient', and it corresponds to the anisotropic form of the classical 'poro-elastic expansion coefficient' ($\bar{B}_{ij}$ is not the inverse of B_{ij}). To sum up, equation (2a) expresses the stress–strain relation under pressure coupling, while equation (2b) is a formulation of the reciprocal strain–stress relation under the same pressure coupling.

- The hydro-mechanical relation expressing water production $\Delta\xi$ (m^3 of water m^{-3} of clay rock) in terms of water pressure variations Δp (via the Biot modulus M) and in terms of the global strain (ε_{ij}) of the poro-elastic medium.

$$\Delta\xi = B_{ij}^{\mathrm{MC}}\varepsilon_{ij} + \frac{1}{M_{\mathrm{MC}}}\Delta p \qquad (3a)$$

where strain tensor is defined as the symmetric part of the gradient of displacement:

$$\varepsilon_{ij} = \left(\frac{\partial u_i}{\partial u_j} + \frac{\partial u_j}{\partial u_i}\right) \Big/ 2 \qquad (3b)$$

Equation (3a) relates water production $\Delta\xi$ to strain and pressure, at any fixed point (x, y, z) in space. The variations in time from an initial reference state are represented by the symbol Δ (as in $\Delta\xi$ and Δp). Note: the strain (ε_{ij}) also contains implicitly a time variation of the displacement vector (u_i), which could also be written equivalently (Δu_i).

- Finally, the water production $\Delta\xi$ also appears in the water flow equation that enforces mass conservation of the moving fluid. This conservation equation takes the form:

$$\frac{\partial m_{\mathrm{W}}}{\partial t} = -\frac{\partial}{\partial x_j}\{\rho_{\mathrm{W}} Q_j\} \qquad (4a)$$

where $\Delta m_{\mathrm{W}} = \rho_{\mathrm{W}}\Delta\xi$ (w representing water).

The equation on the left involves the negative divergence of the mass flux of water ($\rho_{\mathrm{W}} Q_i$). The water flux density vector Q_i (($m^3\ s^{-1}$) m^{-2}) is expressed by an equivalent Darcy's law, which relates linearly water flux to pressure gradient at macroscopic scale via an equivalent permeability tensor k_{ij} (m^2) (and the dynamic viscosity of water μ_{W}):

$$Q_i = -\frac{k_{ij}^{\mathrm{MC}}}{\mu_{\mathrm{W}}}\frac{\partial(p + \rho_{\mathrm{W}} g z)}{\partial x_j} \qquad (4b)$$

This can be simplified in some cases as follows, in terms of hydraulic conductivity K_{ij} ($m\ s^{-1}$), using a reference value for ρ_{W}:

$$Q_i = K_{ij}^{\mathrm{MC}} J_j = -K_{ij}^{\mathrm{MC}}\frac{\partial((p/\rho_{\mathrm{W}}^0 g) + z)}{\partial x_j} \qquad (4c)$$

Inserting the water production term $\Delta\xi$ of equation (3a) and the macroscale Darcy law (equation 4b, c) in the mass conservation equation of the moving fluid (equation 4a) finally closes the entire system of equivalent (upscaled) continuum equations for hydraulics, mechanics and hydro-mechanics. Concerning fluid production, see also Coussy (1991), among other authors.

In the remainder of this work, we focus on mechanics and coupled hydro-mechanics, and we assume that the hydraulics upscaling has already been calculated. However, for the sake of completeness, we will also give a brief comparative outline of various upscaling methods for hydraulics and hydro-mechanics in fractured porous media (see below).

Upscaling method for hydro-mechanics: superposition and coupling

As explained in a previous section, all the equivalent tensorial coefficients (stiffnesses, compliances, coupling coefficients) were calculated in this work by the superposition method, an upscaling technique that takes into account the given geometric structure of the damaged fractured rock (geometry of cracks), as well as the local microscale properties of the fractured rock under various assumptions (quasi-elastic crack with given apertures and normal/shear stiffnesses, isotropic elastic porous matrix, etc.). Figure 2 shows a rough schematic of the fractured porous matrix at the microscale (both the pores of the rock matrix and the cracks are assumed to be filled with water).

It is not the purpose of this paper to give a full detailed account of the mathematical upscaling theory used in this work; however, the interested reader may consider the following discussion and the cited references concerning the mathematical bases of this approach.

Hydraulic upscaling and equivalent macro-permeability tensor. Concerning *hydraulic upscaling*, the reader is referred to Ababou *et al.* (2011): that paper contains a detailed description of the flux superposition method for obtaining an equivalent Darcy permeability, or hydraulic conductivity (K_{ij}). The permeability upscaling method was applied to the same site as in the present work (gallery GMR of the Meuse/Haute-Marne URL), using the same synthetic geometric structure of fractures (the near-wall statistical fractures were fitted to hydraulic conductivity measurements).

For the sake of completeness, let us give a brief outline of permeability upscaling calculations by the flux superposition method. The principle of

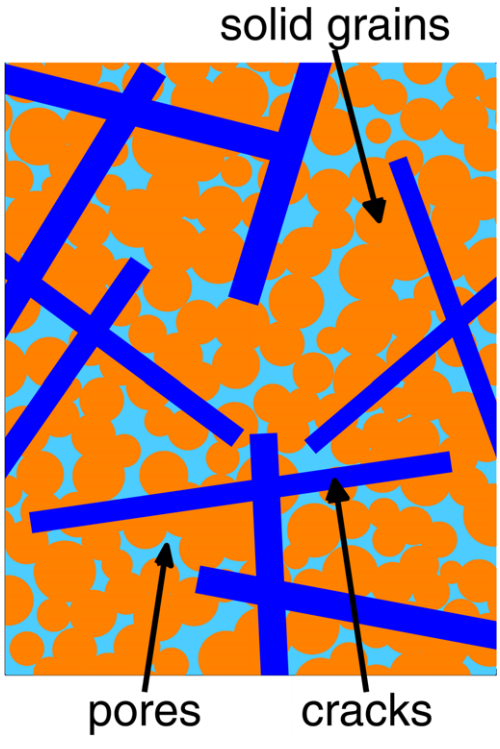

Fig. 2. Micro-scale schematic of the matrix solids (orange circles (grey in print version)), matrix pores (light blue background (light grey in print verison)) and planar cracks (dark blue bars (dark grey in print version)).

the methods is similar for hydro-mechanics, where a tensorial strain superposition is applied (with specific procedures for accounting for stress–pressure–fluid production coupling).

In the fractured porous medium, the local flow is assumed to be governed by the isotropic form of Darcy's law in the porous matrix, and by Poiseuille law in the plane of the cracks. This yields for each crack a 'cubic law', that is, the flow rate in each crack is proportional to the power 3 of its aperture. Upscaling the dual medium (the permeable matrix and cracks) based on a generalized form of the flux superposition method yields a tensorial Darcy law (equation 4a) with an 'equivalent conductivity tensor' (K_{ij}). The latter incorporates the matrix permeability, the hydraulic effects and geometric structure of cracks (apertures, planar sizes, etc.): see Ababou *et al.* (2011). When matrix permeability goes to zero, the resulting K_{ij} is similar to that of Oda & Hatsuyama (1985) and Oda (1986) without Oda's connectivity factor.

Mechanical upscaling. Mechanical upscaling (without hydro-mechanical coupling) is essentially based on the superposition of local strain values ε_{ij}, similar to the superposition of local fluxes in hydraulics. This approach leads, first, to upscaling the compliance coefficients. The equivalent compliance tensor (resulting from strain superposition) contains, essentially, weighted arithmetic averages of local matrix and crack compliances (although this is a rather simplified description of the full expressions).

Second, the upscaled stiffness tensor is obtained as a fourth-rank tensorial inverse of the upscaled compliance tensor. As a consequence, upscaled stiffnesses can be viewed essentially as weighted harmonic averages of local matrix and crack stiffnesses (in a general tensorial sense).

Coupled hydro-mechanical upscaling. The method is again based on the superposition of local strains, but we assume this time that there is a local stress–pressure coupling in each crack, and at each location within the porous matrix. The local H-M coupling in the water-filled cracks is based on Terzaghi's (1936) effective stress concept (equivalent to taking a Biot coefficient equal to one in each crack: $B_C = 1$). The local H-M coupling within the saturated porous rock matrix is either disregarded (cf. hypothesis 'iii.a' in Table 3), or fully taken into account through a matrix Biot coefficient B_M between 0 and 1 ($B_M \approx 0.5–0.6$ from experimental evidence).

The latter result, taking into account Biot coupling in the porosity of the matrix as well as in the cracks, is the more interesting one. Nevertheless, we want to conserve the results obtained both with and without H-M coupling in the matrix for the purpose of analysis (decomposition of coupling effects owing to the cracks v. those owing to the porous matrix).

Technically, and mathematically, the upscaling of hydro-mechanical couplings in the dual matrix–crack medium is a little complex; the resulting upscaled coefficients (B_{ij}, M) contain contractions of fourth-rank tensors, and cannot be described as simple averages except for special cases (the details of the general calculation remain beyond the scope of this paper).

For more details on the strain superposition method for both mechanics and coupled hydro-mechanics under various hypotheses, the reader is referred to, Cañamón *et al.* (2007, 2009); Cañamón (2009) and Ababou *et al.* (1994*a*, *b*). The present paper constitutes a natural generalization, and also a different application, of the latter works. Let us briefly compare the above-cited works with the present work, and particularly, let us point out what simplifying hypotheses have now been relaxed in the present work: compared with the previous cited works, the hydro-mechanical role of the

permeable porous matrix is fully taken into account. The pressure coupling terms calculated in the present paper can fully take into account the contribution of the water-filled porous matrix as well as the water-filled cracks.

However, for simplicity and for comparison purposes, when displaying the spatial distributions of ellipsoids representing the coupling coefficients (B_{ij}, M), these are calculated for the sole contribution of the cracks, and in that case, they are labelled ($B_{ij}^{(0)}$, $M^{(0)}$). On the other hand, all the global and annular values of (B, M) given in the text and tables include the complete coupling effects of both cracks and matrix.

Spatial averaging procedures

It should be emphasized that the theoretical upscaling method can be used, technically, for obtaining different types of upscaled coefficients using various spatial averaging 'supports' and various scales (e.g. cubic or rectangular voxels of various sizes, annular regions of various thicknesses).

Indeed, in this work, several distinct versions of the upscaled continuum coefficients are calculated, as mentioned earlier. The equivalent coefficients are obtained either as 3D fields distributed in (x, y, z), or as 2D fields distributed in a transverse cross-section (y, z) orthogonal to the axis of the gallery (x). Other types of averages will also be presented, such as the annular average over a cylindrical annular shell at various radial distances from the wall of the gallery. Furthermore, 'global' values of the coefficients are calculated by taking the annular domain to be as thick as the entire damaged and fractured zone (about 4 m thickness around the wall of the gallery). These different versions of the upscaled continuum coefficients (3D, 2D, annular, global) can be computed by two possible alternative methods:

(1) *Direct upscaling* – the term 'direct upscaling' designates the usual upscaling procedure based on strain superposition (as described in previous sections), starting with discrete matrix–crack hydro-mechanical laws at the microscale, and upscaling them to equivalent continuum laws at the desired scale (meso or homogenization scale). The upscaling domain may be anything here: a 3D voxel, a parallelepiped box, an annular shell or a moving spherical window, etc.

(2) *Sequential upscaling* – here is an example of 'sequential upscaling' that was used in this work. The transverse distributions of '2D upscaled' quantities were obtained, first, by calculating the '3D upscaled' quantities on a grid of cubic voxels (each voxel is a subdomain), and second, by applying axial averaging operations (compatible with the upscaling theory) to obtain '2D upscaled' quantities over a transverse planar grid of pixels. Note: each pixel represents an elongated parallelepiped having the same length as the stretch of gallery considered ($L = 20$m here).

These different ideas are illustrated in Figure 3.

Equivalent isotropic scalar coefficients at annular and global scales

One more word of caution is needed concerning the interpretation of 'global scale' and 'annular scale' equivalent coefficients (see results in the next sections on global and annular upscaling, and see Tables 3–6).

- Annular and global scale coefficients are obtained from the tensorial superposition method applied to a cylindrical annular shell. When the annular shell has the thickness of the EDZ, we call the resulting tensorial coefficients 'EDZ-scale' coefficients. For annular shells of smaller thickness (e.g. 0.5 m), we obtain an annular tensorial coefficient for each various shell (the shells being located at various radial distances from the drift wall).
- At this stage, the calculated annular coefficients remain generally tensorial (more precisely, we obtain in this way annular or global values of R_{ijkl}, C_{ijkl}, B_{ij} and M).
- However, the point we want to make is that the choice of annular upscaling leads naturally to a loss of information on the anisotropic structure of the coefficients (except for '*M*', which is in essence a scalar). For this reason, the global and annular results presented in the next section (Tables 3–6) are shown as scalars rather than tensors. The scalar values are isotropic equivalents obtained with the '*isotropization*' procedure defined in Appendix 1. There is only one exception: the shear compliance diagonal values S_{jj} are given for various annular shells, in Tables 4–6. This information is only used to show one example of annular coefficients without *isotropization*.

In summary, most annular and global quantities calculated in this work based on tensorial superposition are finally evaluated as equivalent isotropic scalar properties (Appendix 1). On the other hand, local scale continuum equivalent coefficients are still evaluated as full tensors, to be visualized in the next section as ellipsoids distributed around the gallery. The term 'local scale'

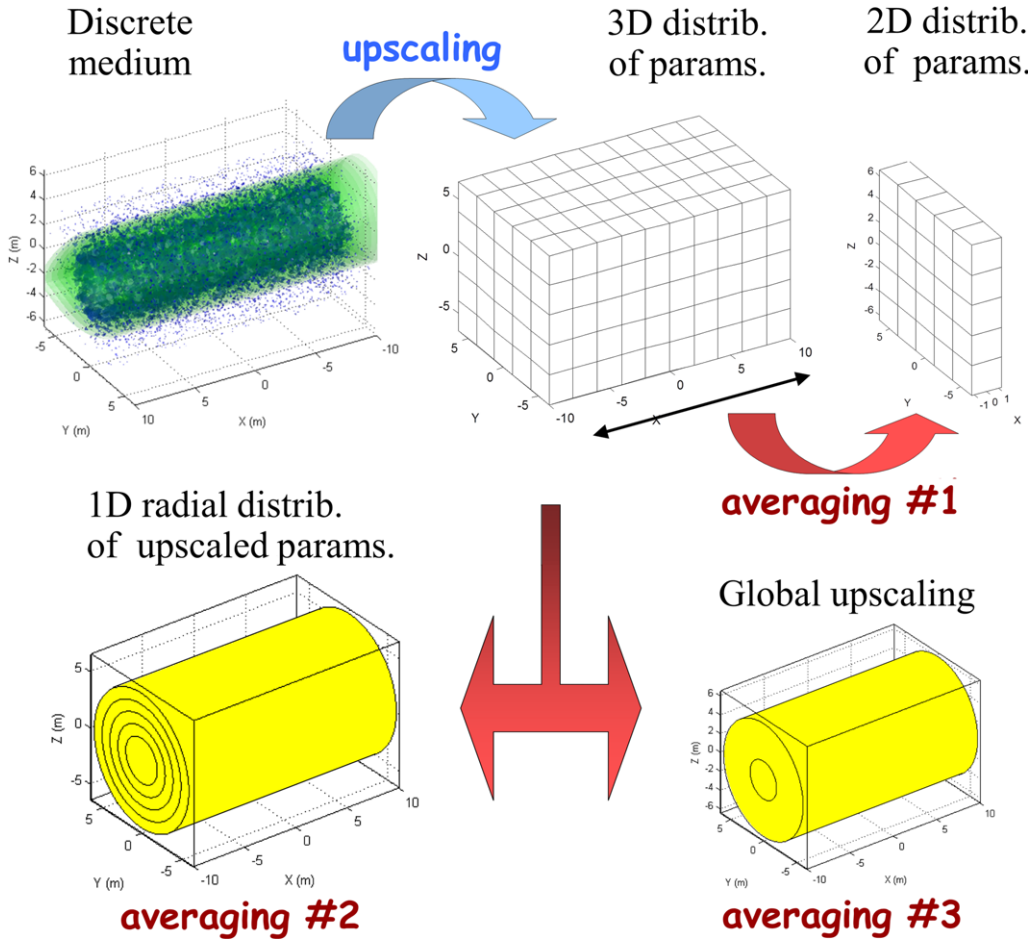

Fig. 3. Upscaling and averaging, leading to 3D, 2D or radially distributed, equivalent continuum upscaled coefficients (compliances, stiffnesses, coupling coefficients).

corresponds to the case where the two transverse dimensions of the averaging domain are smaller than drift diameter (e.g. cubic voxels of size $0.5 \ll 4.0$ m).

Inputs, results, analyses: equivalent 'H-M' coefficients

Inputs, outputs and post-treatment of hydro-mechanical upscaling

Inputs/outputs of upscaling and numerical values of input parameters. Tables 1 and 2 present two types of information:

(1) A list of inputs/outputs – the 'input' parameters (porous rock matrix and cracks) and the 'output' coefficients to be obtained by implementing the upscaling procedure (set of tensorial upscaled Hydro-Mechanical coefficients); and

(2) A list of numerical values of the basic hydro-mechanical and geometrical input parameters, such as matrix porosity, crack aperture, crack stiffnesses (normal and shear), matrix Young's modulus, Poisson's ratio, etc.

Hydro-mechanical coefficients (B, M) *for the rock matrix: experimental evidence.* Some of the parameters of Tables 1 and 2 (particularly for the rock matrix) were selected by comparison with the internal databank of ANDRA (see for instance ANDRA 2005*a*), and by comparison with other works in the literature, as explained below. The mean value of the Biot coefficient *B* over different layers in the Callovo-Oxfordian (between

Table 1. *Input and output parameters for the upscaling process: lists of input parameters and output coefficients (hydro-mechanical)*

Parameters	Crack (c)	Porous matrix	Equaivalent continuum
Hydraulic	$a^{(c)}$, $n_1^{(c)}$ (Poiseuille)	K_M	K_{IJ}^{MC}
Mechanic	$K_N^{(c)}$, $K_S^{(c)}$	E_M, ν_M	R_{ijkl}^{MC}
Hydro-mechanical	$B^{(c)}=1$ (Terzaghi)	B_M, M_M	B_{ij}^{MC}, M^{MC}

depths 400–500 m roughly) was calculated by Cosenza *et al.* (2002) in their table 1. They obtained the value $B \approx 0.4$ (range: $B = 0.37$–0.42) *and* observed that this value is close to that obtained directly by hydro-mechanical tests in other works, and they quote in particular the tri-axial tests of Coste *et al.* (1999), who obtained $B = 0.36$ '*for the same claystone*', while other authors like Vincké *et al.* (1997) obtained higher values from $B = 0.4$ up to 0.8, also '*for the same claystone*'. Other data obtained *in-situ* at the Meuse/Haute-Marne URL seem to point to the value $B \approx 0.6$ for the 'intact' rock matrix (although small fissures cannot be avoided on rock matrix samples extracted *in-situ*). For these reasons, we have taken $B_{\text{MATRIX}} \approx 0.5$ for the intact rock matrix in this study.

Concerning the Biot modulus '*M*', based on Cosenza *et al.* (2002), their calculated Biot modulus is about $M \approx 8$ GPa (range: $M = 7.69$–8.36 GPa in their table 1). There are few (if any) other more direct *in-situ* measurements of the Biot modulus of this claystone in the literature. We will take therefore $M \approx 8$ GPa or so, for the Biot modulus of the intact claystone matrix. We have verified that this value is close to that which can be obtained theoretically (from Biot's isotropic theory of granular materials) for the intact rock matrix using reasonable microscale parameters (final value: $M_M = 8.68$ GPa in our Table 3).

Ellipsoidal representation and visualization of upscaled tensorial coefficients. Recall that most of the H-M coefficients are tensorial (except for the scalar Biot modulus '*M*'). For this reason, we use an algebraic interpretation that allows us to represent any positive definite symmetric second-rank tensor, such as K_{ij} and B_{ij}, as a 3D ellipsoid. For example, the tensorial version of Darcy's law (with hydraulic conductivity tensor K_{ij}) can be used to define a directional conductivity along the gradient direction (K_{grad}) and a directional conductivity along the flux direction (K_{flux}); it is then

Table 2. *Input and output parameters for the upscaling process: numerical values of input parameters used for obtaining upscaled hydro-mechanical coefficients*

Radius and length of the stretch of drift	Drift radius: $R = 2$ m, Axial length of drift stretch: $L = 20$ m
Apertures of planar disc fissures (small fractures)	$a_{\text{FISSURES}} \approx 5 \times 10^{-5}$ m near the wall, decreasing rapidly away from wall
Diameter of planar disc fissures (small fractures)	$d_{\text{FISSURES}} \approx 0.8$ m near the wall, decreasing rapidly away from wall
Density of planar disc fissures (small fractures)	$(\rho_{32})_{\text{FISSURES}} \approx 6.11\ \text{m}^2\ \text{m}^{-3}$ near the wall, decreasing rapidly away from the wall
Aperture of curved 'chevron' fractures	$a_{\text{FRACT/CHEVRON}} \approx 1 \times 10^{-4}$ m $= 100\ \mu$ constant
Size of curved 'chevron' fractures	Horizontal extension: 4 m Vertical extension: 4 m
Density of large curved 'chevron' fractures	$(\rho_{1D})_{\text{FRACT/CHEVRON}} = 2/\text{m}$, periodic along the drift axis
Normal specific stiffness of planar cracks	$K_N = 1 \times 10^{10}$ Pa $= 10$ GPa
Shear specific stiffness of planar cracks	$K_S = 1 \times 10^{9}$ Pa $= 1$ GPa
Rock matrix Young's modulus	$E_M = 5 \times 10^{9}$ Pa $= 5$ GPa
Rock matrix Poisson ratio	$\nu_M = 0.30$
Rock matrix porosity	$\theta_M = 0.14$

Table 3. *Global equivalent coefficients: hydro-mechanical coefficients of the fissured and fractured claystone, upscaled at the global scale of the 4 m thick damaged zone, and isotropized*

Table parameter (global)	Intact matrix	Matrix and fissures	Matrix and fissures and chevron fractures
Young's modulus, E (GPa)	5.0	3.0	1.31
Poisson ratio, ν	0.30	0.34	0.37
Shear modulus, G (GPa)	3.85	2.24	0.96
Biot coefficient, B (iii.a)	0	0.113	0.281
Biot coefficient, B (iii.b)	0.50	0.556	0.641
Biot modulus, M (GPa) (iii.a)	∞	36.8	14.8
Biot modulus, M (GPa) (iii.b)	8.68	7.47	6.25

Hypothesis 'iii.a' ignores H-M coupling within the matrix (coupling is due only to cracks), hypothesis 'iii.b' includes both the coupling role of the porous matrix and of the cracks
Note: 'matrix' values are also shown in this table. The 'matrix' is the intact porous rock; the 'fissures' are the statistical planar disc fissures (i.e. small fractures); the 'chevrons' are the large curved fractures organized in a chevron pattern along the drift axis.

possible to show that the polar plots of $\sqrt{(1/K_{\text{grad}})}$ and of $\sqrt{(K_{\text{flux}})}$ both describe an ellipse in 2D or an ellipsoid in 3D (Bailly 2009: chapter 10; Bailly *et al.* 2011). However, for simplicity, we have chosen here to represent with ellipsoids the matrix quantities A_{ij} (i.e. specifically K_{ij}, S_{ij} or S_{IJ}, B_{ij}, etc.), such that the three principal axes of an ellipsoid indicate the directions of the three eigenvectors of matrix A_{ij}, and the three principal radii of the ellipsoid are equal to the corresponding three eigenvalues of matrix A_{ij} (as in Ababou *et al.* 2011).

Accordingly, at any spatial position (or for any subdomain), the upscaled second-rank tensor B_{ij} (Biot coefficient) is represented directionally by an ellipsoid, just like the upscaled hydraulic conductivity K_{ij} in the work of Ababou *et al.* (2011). Thus, strongly anisotropic B_{ij}s are indicated by strongly elongated and/or flat ellipsoids (strongly prolate like a rugby ball, strongly oblate like a saucer, etc.). The Biot modulus M is plotted as a sphere, whose radius indicates the magnitude of M. Indeed, any scalar quantity like 'M' can be expressed equivalently as an isotropic (spherical) tensor, which can be represented by a sphere.

Finally, the purely mechanical coefficients of compliance (C_{ijkl}) and stiffness (R_{ijkl}) are higher-order tensors (fourth-rank). This makes it more difficult to represent their spatial distribution. The interested reader is referred to other possible representations in the literature, some of them based on Kelvin's decomposition of fourth-rank elastic tensors: Mehrabadi & Cowin (1990); Basser & Pajevic (2007); Pouya (2007, 2011); see also Charlez (1991).

In the present work, we have chosen to reduce the amount of information, and to display only some parts of the C_{ijkl} and R_{ijkl} tensors. For example, the stiffness tensor R_{ijkl} can be described (partially) via two 3×3 matrices – each of which can be represented by ellipsoids:

- 'normal stiffness' matrix N_{IJ} containing stiffness coefficients R_{1111}, …, R_{3333}, R_{1122}, etc;
- 'shear stiffness' matrix S_{IJ} containing stiffness coefficients R_{2323}, …, R_{2312}, R_{1313},etc.

Therefore, the upscaled mechanical coefficients, such as 'normal stiffness' N_{IJ} and 'shear stiffness' S_{IJ}, can be represented by ellipsoids. In fact, the shear matrix ellipsoid (S_{IJ}) is easier to interpret, as it reduces to a sphere in the case of isotropic shear stiffnesses (whereas the normal ellipsoid N_{IJ} does not reduce to a sphere in the case of isotropic elasticity). We focus in this paper on the shear submatrix S_{IJ} (see also Table 6 and Appendix 1).

Post-calculation of equivalent 'isotropized' scalar coefficients. In order to remedy some possible interpretation problems with these ellipsoids (particularly for the so-called 'normal' ellipsoids of stiffnesses and compliances), it was decided to extract a set of more 'classical' mechanical coefficients (E, K, λ, μ, ν) from the full fourth-rank compliance and stiffness tensors and similarly for the H-M coupling coefficients (B_{ij}, M), which become (B, M) after *isotropization*. These calculations were performed using adequate contractions of second- and fourth-rank tensors, based on the definition of spherical quantities similar to the definition of a spherical bulk stiffness K in isotropic elasticity. This is summarized in Appendix 1 (a fully detailed algebraic implementation of these concepts for non-isotropic/non-orthotropic fourth-rank elasticity would be beyond the scope of this paper).

The resulting scalar coefficients (E, K, λ, μ, ν, B, M) should be considered as 'isotropized' versions of

the upscaled tensorial coefficients (C_{ijkl}, R_{ijkl}). Each scalar can then be represented as a spatial distribution (if upscaled locally), or else it can be computed as a global quantity (if upscaled at the macroscale of the entire damaged/fractured zone). For example, numerical values of global isotropized coefficients (E, K, λ, μ, ν, B, M) is presented in Table 3.

Note: E = Young modulus; K = bulk spherical modulus; (λ, μ) are the Lamé moduli (in particular μ is the shear modulus); ν is the Poisson ratio; and finally (B, M) are the coupling coefficients (Biot coefficient B, and Biot modulus M).

3D upscaling: distribution of H-M coefficients on a cartesian grid (voxels)

In this section, we display graphically the 3D upscaled tensorial coefficients around the drift, as spatially distributed ellipsoids located on a cartesian grid of voxels (x_{IJK}, y_{IJK}, z_{IJK}).

Recall that the upscaled coefficients are generally second- and fourth-rank tensors, to be represented via 3×3 ellipsoids. The total 3D domain of damaged and fractured rock, in our case, is a 20 m stretch of gallery, with transverse size 13 × 13 m (comprising the 4 m diameter drift). The chosen size of the cubic voxels (subdomains) is 0.50 m. For these reasons, displaying the spatial distributions of tensorial coefficients in 3D space over the entire domain can be cumbersome. Several 3D views would be needed in order to clearly see all the 3×3 ellipsoids in (x, y, z) space. Therefore, to save space, we show only the *first transverse layer* of the 3D distribution, that is, the (Y, Z) plane with $X \in [-10.0\text{ m}, -9.5\text{ m}]$. This gives an idea of the 3D heterogeneity of upscaled coefficients inside the damaged/fractured zone around the drift.

The results are displayed in Figure 4, showing the first transverse layer of the 3D upscaled tensors (3×3 ellipsoids) for several types of coefficients (normal compliance N_{ij}, shear compliance S_{IJ}, Biot coefficient B_{ij}, and inverse Biot modulus $1/M$).

2D upscaling: distribution of H-M coefficients on a transverse grid of pixels

In this section, we display graphically the 2D upscaled tensorial coefficients around the drift, as spatially distributed ellipsoids located on a cartesian grid of pixels (y_{JK}, z_{JK}): see Figure 5. Note that, although their spatial distribution is 2D, these tensorial coefficients are still represented by 3×3 ellipsoids, so their '3D anisotropy' can still be seen by looking at the ellipsoids (e.g. ellipsoids of shear compliance S_{ij} and Biot coefficient B_{ij}).

In comparison with the 3D spatial distributions shown earlier, the 2D upscaled coefficients appear less anisotropic, and less variable in space (particularly near the wall). This effect was expected: it is due to the additional smoothing induced by averaging along the axis of the drift (compared with the 3D results which were not axially averaged). The advantage of the 2D transverse representation is that it offers a more synthetic view of the upscaled coefficients around the drift, but at the price of some loss of information (anisotropy and heterogeneity have been significantly smoothed out by axial averaging).

Global upscaling: H-M coefficients on a 4 m thick annular cylinder (EDZ)

The strain superposition upscaling procedure was used to calculate the tensorial coefficients at the global scale (macroscale) of the entire EDZ, that is, the entire damaged zone around the 20 m long stretch of the drift. The 'global' upscaling domain, in this case, is the EDZ, defined as the 20 m long cylindrical annular region of thickness 4 m around the drift (EDZ thickness is about one diameter around the drift, and the drift radius, R, is 2 m).

Once the global tensors have been calculated by the tensorial superposition method (R_{ijkl}, C_{ijkl}, B_{ij}, M), they are processed algebraically to obtain 'equivalent isotropic' scalar quantities (E, K, λ, μ, ν, B, M), as explained in Appendix 1. These final results, summarized in Table 3, provide a simplified synthetic view of the global properties of the fissured and fractured claystone around the drift. In particular, consider the Biot modulus (M). Note that 'M' can be interpreted as the *stiffness of the coupling* between pressure variations and fluid production. It can be seen, as expected, that the global value of the coupling stiffness 'M' is reduced as more cracks are 'added':

$$M_{\text{M}} = 8.68\,\text{GPa} > M_{\text{M+Fiss}} = 7.47\,\text{GPa} > M_{\text{M+Fiss+FractChevr}} = 6.25\,\text{GPa}$$

Annular upscaling: H-M coefficients on annular domains around the drift: 'near-wall' v. 'far-wall' values, and comparisons with global values

In this section, we present results obtained by upscaling the H-M coefficients over *annular shells*, rather than voxels or pixels. For simplicity, we present here not the full tensorial coefficients, but their equivalent isotropized values (as explained

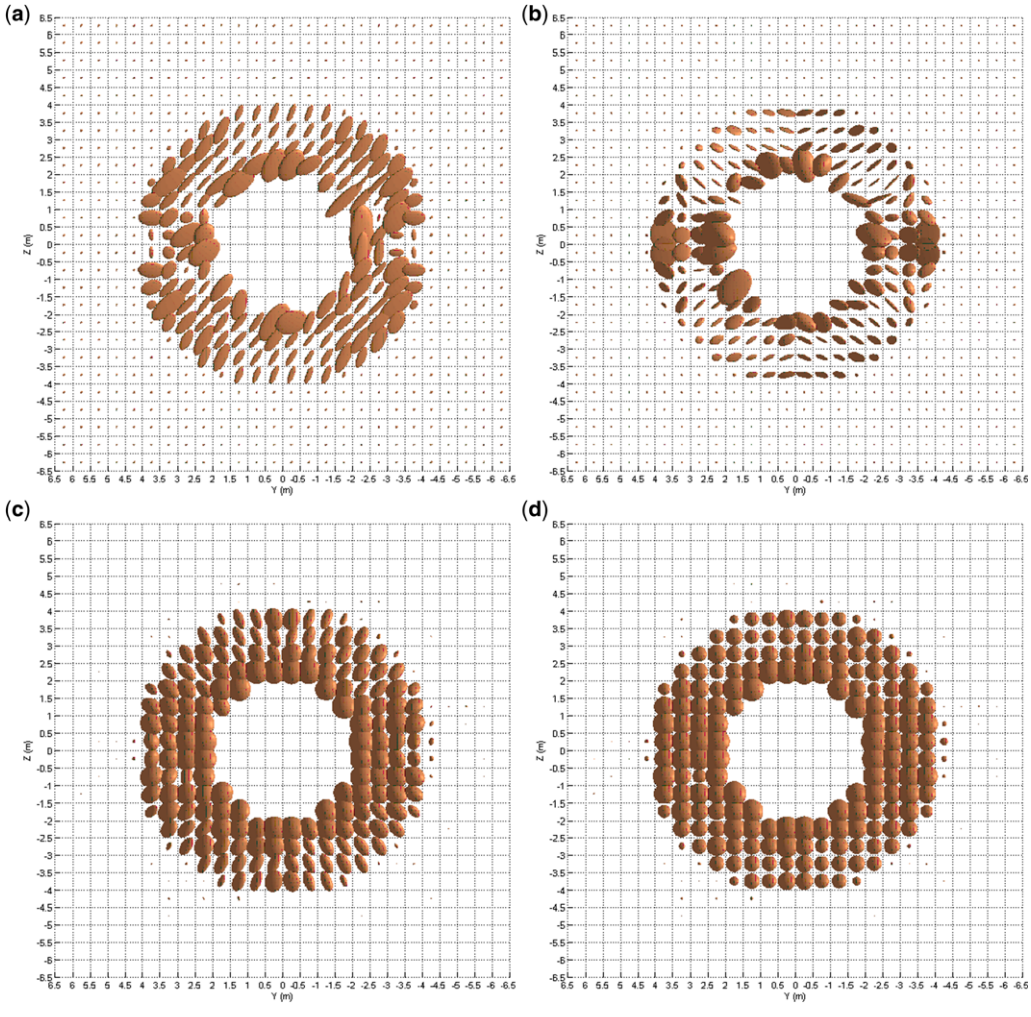

Fig. 4. Frontal views of the 3D upscaled coefficients: (**a**) normal compliance N_{ij}; (**b**) shear compliance S_{ij}; (**c**) Biot coefficient ${B_{ij}}^{(0)}$ (ellipsoids); and (**d**) inverse of the Biot modulus $1/M^{(0)}$ (spheres) in the first transverse layer (Y, Z) with $X \in [-10.0\text{ m}, -9.5\text{ m}]$. These upscaling calculations take into account the porous rock matrix (except for its coupling effects on B_{ij} and M), including the statistical set of fissures (small fractures), and the periodic set of large curved fractures (chevron pattern). For the coupling coefficients ${B_{ij}}^{(0)}$ and $M^{(0)}$, in this figure, hypothesis (iii.a) was used; superscript (0) indicates that the coefficient is calculated *relative* to the sole coupling effects of cracks (fissures and fractures).

in Appendix 1). The resulting scalar values represent coefficients upscaled on annular shells of various thicknesses.

For example, using this technique, we obtain $B \approx 0.90$ near the wall, that is, over a 0.5 m thick annular shell adjacent to the wall ($r \in [2.0\text{ m}, 2.5\text{ m}]$). This value $B \approx 0.90$ should be compared with the global value $B = 0.641$ given earlier at the global scale of the entire 4 m thick and 20 m long stretch of damaged/fractured rock around the drift. It should also be compared with the value $B = B_{\mathrm{M}} = 0.50$ assumed for the intact rock matrix (Table 3).

We show a few more results along these lines in Tables 4–6. The tables describe the radial distributions of several mechanical and hydro-mechanical properties of the damaged claystone. These properties are obtained in two steps: (a) by upscaling the tensorial coefficients on annular cylindrical shells; and (b) by evaluating the resulting *equivalent isotropic* coefficients, at each radial distance from the centre of the drift.

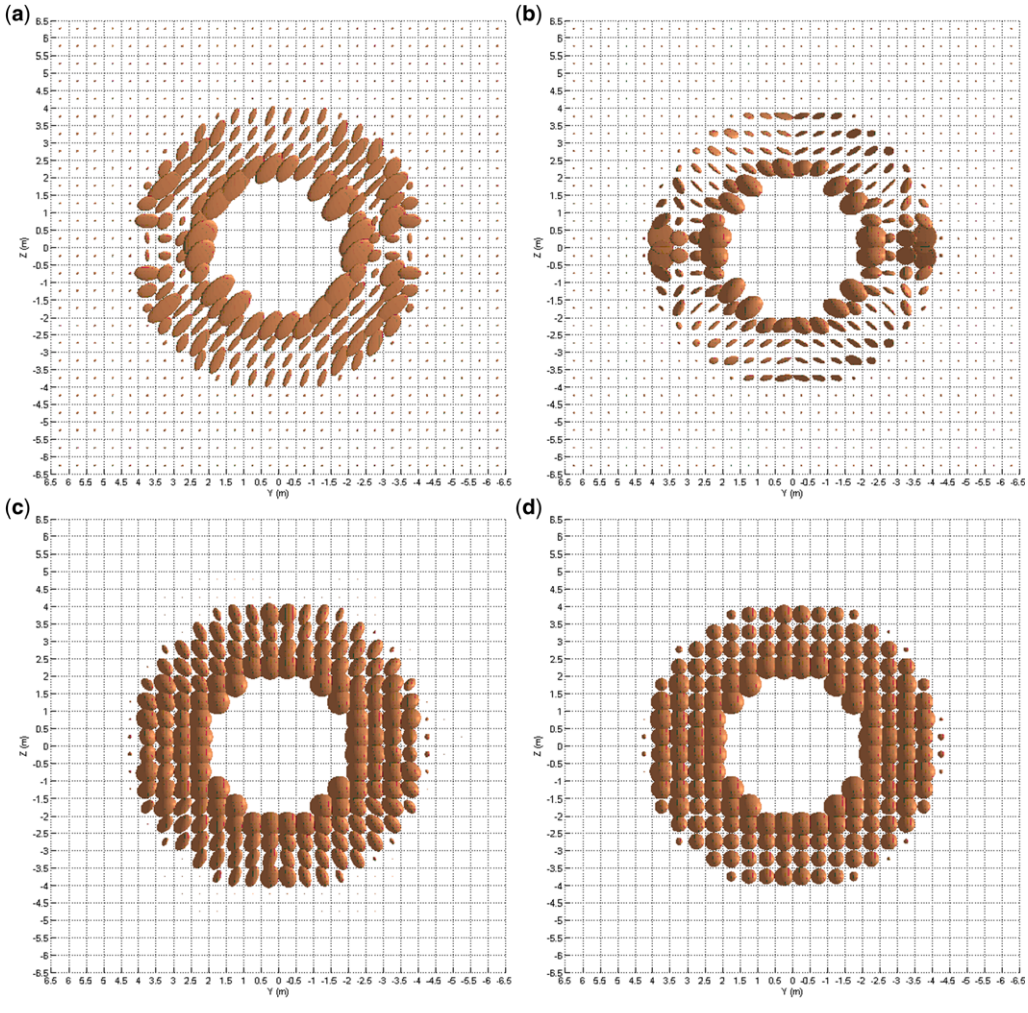

Fig. 5. Transverse 2D distributions (averaged along the X axis) of upscaled coefficients: (**a**) normal compliance N_{ij}; (**b**) shear compliance S_{ij}; (**c**) Biot coefficient $B_{ij}^{(0)}$ (ellipsoids); and (**d**) inverse of the Biot modulus $1/M^{(0)}$, taking into account the porous matrix, the small fractures (fissures) and the large chevron fractures. For the coupling coefficients B_{ij} and M, in this figure, hypothesis (iii.a) was used; superscript (0) indicates values *relative* to the sole coupling effects of cracks (fissures and fractures).

However, we also show the values of a tensorial coefficient (the shear compliance submatrix S_{IJ}) in order to examine its degree of anisotropy v. radial distance: looking at the diagonal values S_{II} (II = 44,55,66), it can be seen that the claystone is not only more compliant but also more anisotropic in the near-wall region (say within 0.5–1.0 m from the wall). On the other hand, the apparent anisotropy of S_{IJ} is not very strong, most probably because of the annular averaging process (see discussion in Section 3.4). The important thing is that shear compliance decreases by a factor 15 or so from near-wall to 4.5 m away from the wall. We will return to a brief discussion on the results of Tables 4–6 in the next section.

Conclusions, discussion and outlook

Conclusions and discussion

The results obtained so far for the upscaled hydro-mechanical properties of the damaged, fissured and fractured claystone around a gallery at the Meuse/Haute-Marne URL site are now summarized and discussed. (Recall that the upscaling considers the porous claystone matrix with embedded cracks

Table 4. *Radial distributions of mechanical and hydro-mechanical equivalent continuum coefficients upscaled on annular shells around the drift (the drift wall is located at $R = 2.0$ m from the drift centre): hydro-mechanical coupling coefficients v. radial distance R (for annular shells with R comprised between R1 and R2)*

R1 m	R2 m	B (Biot coefficient)	M (Biot modulus, GPa)
2.0	2.5	0.8717	6.5015
2.5	3.0	0.7812	6.9262
3.0	3.5	0.7696	6.9818
3.5	4.0	0.7519	7.0718
4.0	4.5	0.5219	8.5102
4.5	5.0	0.500	8.6778
5.0	5.5	0.500	8.6778
5.5	6.0	0.500	8.6778

comprising a set of statistical planar disc fissures, and a set of large curved 'chevron' fractures discretized into triangular patches.)

Global v. local rock properties. At the *global scale* of the damaged zone (4 m thick annular cylinder), the Young's and shear *moduli* are *reduced by a factor 4* compared with the intact rock matrix. The *global* Poisson ratio is not much changed with respect to the matrix value: it is only slightly increased, from 0.30 to <0.40.

On the other hand, at the *local scale*, the stiffness moduli can be *reduced by one order of magnitude* or more in the near-wall region, as shown for instance by comparing annularly upscaled values ($r \approx 2.0$ m-2.5 m) with global values.

Furthermore, looking at the '3D' coefficients, locally upscaled on a grid of cubic voxels (Figure 4 ellipsoids), it is clear that material compliances like the shear compliance matrix S_{IJ}, and the inverse Biot modulus $1/M$, increase significantly near the gallery wall.

This is confirmed by looking at Tables 4–6, where it is also seen that material *anisotropy* also increases significantly near the gallery wall (see the values of S_{II} in Table 6, and see also the '3D' ellipsoids of S_{IJ} and B_{ij} in Figure 4.

Hydro-mechanical coupling coefficients $\mathrm{B_{ij}}$ *and* M *(upscaled results).* The Biot coefficient B and the Biot modulus M are calculated first by taking into account the sole effect of the cracks (hypothesis 'iii.a'), and then by taking into account the complete coupling effects owing to porous matrix as well as cracks (hypothesis 'iii.b').

Looking at the *global* values shown in Table 3 under the more general hypothesis 'iii.b', and comparing these values with those of the intact rock matrix, it is clear that the upscaled Biot coefficient (B) *increases with damage* (while staying below unity, as it should), and that the Biot modulus (M) *decreases with damage*. These results are as expected physically, since damaging and fracturing should weaken the rock.

Extent of the hydro-mechanically damaged zone (based on upscaling results). It is seen here that, for all H-M coefficients (except the permeability, examined in Ababou *et al.* 2011), the 'far-wall' values obtained beyond $R = 4.5$ m coincide with the intact rock matrix properties. Since the radius of the gallery is $R = 2.0$ m, it can be concluded that, according to these upscaling calculations, the hydro-mechanically damaged rock lies in an annular region of thickness 2.5 m around the gallery wall.

Remarks on full tensorial coefficients v. simplified isotropic equivalents. From a theoretical point of view, the proposed upscaling method yields generally non-isotropic/non-orthotropic *tensorial*

Table 5. *Radial distributions of mechanical and hydro-mechanical equivalent continuum coefficients upscaled on annular shells around the drift (the drift wall is located at $R = 2.0$ m from the drift centre): mechanical coefficients (obtained from C_{ijkl}) v. radial distance R*

R1 m	R2 m	E (Young's modulus) (GPa)	μ (shear modulus) (GPa)	ν (Poisson's ratio)
2.0	2.5	0.42694	0.14971	0.4259
2.5	3.0	0.85225	0.30159	0.4129
3.0	3.5	0.69583	0.24379	0.4271
3.5	4.0	0.65671	0.22932	0.4319
4.0	4.5	3.8936	1.4592	0.3342
4.5	5.0	5.0000	1.9231	0.3000
5.0	5.5	5.0000	1.9231	0.3000
5.5	6.0	5.0000	1.9231	0.3000

Table 6. *Radial distributions of mechanical and hydro-mechanical equivalent continuum coefficients upscaled on annular shells around the drift (the drift wall is located at R = 2.0 m from the drift centre): shear compliance tensor S_{ij} (principal components) v. radial distance R*

R1 m	R2 m	S_{44} (Pa^{-1})	S_{55} (Pa^{-1})	S_{66} (Pa^{-1})
2.0	2.5	1.8859×10^{-9}	2.1661×10^{-9}	1.5341×10^{-9}
2.5	3.0	9.0955×10^{-10}	1.2262×10^{-9}	7.0979×10^{-10}
3.0	3.5	7.4276×10^{-10}	1.0856×10^{-9}	7.8636×10^{-10}
3.5	4.0	7.0106×10^{-10}	9.1224×10^{-10}	8.0620×10^{-10}
4.0	4.5	1.5526×10^{-10}	1.5485×10^{-10}	1.5815×10^{-10}
4.5	5.0	1.3000×10^{-10}	1.3000×10^{-10}	1.3000×10^{-10}
5.0	5.5	1.3000×10^{-10}	1.3000×10^{-10}	1.3000×10^{-10}
5.5	6.0	1.3000×10^{-10}	1.3000×10^{-10}	1.3000×10^{-10}

stress–strain–pressure relations, represented by tensorial coefficients of rank up to 4.

As explained earlier, the mechanical tensors of rank 4 (R_{ijkl}, C_{ijkl}) were reduced to 3×3 'normal' and 'shear' submatrices representing the upscaled stiffness and compliance tensors of rank 4. These submatrices were then visualized as spatially distributed ellipsoids on the top parts of Figures 4 and 5 (admittedly, shear compliance ellipsoids are easier to interpret than normal compliances). For second-rank tensors, their representation via ellipsoids is more direct and straightforward. The symmetric tensor B_{ij} is shown as an ellipsoid (like the permeability K_{ij} in other works), and the scalar M is shown as a sphere representing the spherical tensor $M\delta_{ij}$: see the bottom parts of Figures 4 and 5.

Finally, recall that the *scalar values* of upscaled coefficients, like those given in Tables 4 and 5, were obtained by 'post-processing' the *tensorial* stress–strain–pressure relations with their second- and fourth-rank tensorial coefficients. Indeed, we have exploited an algebraic theoretical formulation, which has allowed us to define consistently the *equivalent isotropic coefficients* for these laws. For a second-rank tensor like B_{ij}, one way to obtain the isotropic equivalent is to take the spherical part: $B = \mathrm{Tr}(B)/3 = B_{kk}/3$ (however the complete theory is more involved and will not be detailed here).

Remarks on the validity of results. The equivalent continuum H-M coefficients obtained in this work depend on two sets of assumptions and approximations: (a) assumptions on the geometric structure and local properties of the fractured rock (cracks and porous matrix); and (b) approximations and hypotheses linked to the method of upscaling for the matrix–crack medium (here the superposition method).

First, let us recall that the 'geometric model' used for generating the structure of the fractured rock around the gallery, was defined in a previous paper (Ababou *et al.* 2011) where hydraulic upscaling was studied for the same site and the same gallery. In particular, let us point out the following:

- The fracture system in the EDZ was composed of two subsets – the periodic set of large curved chevron fractures, and a statistical set of smaller planar fractures.
- The curved chevron fractures were modelled deterministically based on direct observations of large fracture traces on different planes (exploration ditches); a 3D parametric surface model was then adjusted (a generalized conoid having no axial symmetry).
- The probabilistic/geometric structure of the statistical set was validated based on comparisons of upscaled v. borehole permeability profiles (*in-situ*). This served in particular to adjust the radial inhomogeneity of statistical fracturing in the near-wall region.

In this paper, we assume that the geometric structure is reasonably well established from these previous tests (Ababou *et al.* 2011). The assumed geometric structure of the fractured rock in the EDZ was partially validated by hydraulic measurements and by observation of large fracture traces in that work. That is why we have conserved the same sets of fractures in the present study of hydro-mechanical upscaling.

Second, the superposition method of upscaling does not deliver exact results except in special cases. However, it is fast to implement, it is flexible in terms of the choice of averaging support, and it is able to convey the *anisotropic* and *coupled* hydro-mechanical response of a porous fractured rock. Other upscaling methods may not be as flexible and fast, and they too suffer from defects, approximations and limited range of applicability (as discussed briefly in previous sections).

On the other hand, as shown from the previous discussion of results, our equivalent continuum H-M coefficients match quantitatively some of the

available observations, and they behave qualitatively as expected with the degree of fracturing.

Outlook

In future, we will present the mathematical upscaling theory which has led us to the above-discussed results. A brief description of the theoretical upscaling method based on strain superposition was provided earlier, along with appropriate references. The *upscaling hypotheses* were clearly listed, and it was noted that the current results on coupled hydro-mechanics were obtained under the most general hypothesis (i.e. under hypothesis 'iii.b' rather than 'iii.a'; see Section 3.2 and results of Table 3).

Note that we have obtained $B \approx 0.90$ for the 'near-wall' value of the Biot coefficient (upscaled over a 0.5 m thick annular shell adjacent to the wall). This value should be compared with the global value $B = 0.641$ for the entire 4 m thick global domain. More generally, the reader can compare the radial distributions of stiffnesses and coupling coefficients shown in Tables 4–6 with the global values shown in Table 3.

We plan to complete these results and analyses (*upscaled H-M coefficients of the damaged and fractured clay stone*) by implementing the upscaling method on a variety of other '*spatial supports*', for example, smaller size voxels in 3D and annular shells of smaller thicknesses. In addition, we plan to obtain continuously distributed upscaled parameters using *moving windows* (rather than fixed subdomains or partitions): see for instance the upscaled radial permeability profiles $K(r)$ obtained by Ababou *et al.* (2011). Similarly, it is expected that the current hydro-mechanical upscaling will allow us to obtain properties such as K (bulk stiffness) and B (spherical Biot coefficient) along 'numerical boreholes'.

Other *extensions* of our upscaling method are currently being considered for hydro-mechanical processes. The method, based on superposition of strains and fluxes, can be extended to account for: (a) weakly non-elastic/non-reversible deformation behaviour of the discrete cracks (a brief review of such effects can be found in Oda (1986) and references therein); and (b) retro-active 'feedback' effects of stress and strain on the upscaled properties themselves, such as hydraulic conductivity K_{ij} (which is very sensitive to crack apertures), but also other hydro-mechanical properties (compliances C_{ijkl}, and coupling coefficients B_{ij} and M). Our current theoretical developments and extensions indicate that the Biot modulus 'M' is indeed most sensitive to crack apertures and normal stiffnesses. Therefore it is expected that 'M' is quite sensitive to mechanical feedbacks owing to aperture variations. Note: the tensorial feedback effect of strain–stress on permeability k_{ij} was previously described theoretically in Ababou *et al.* (1994*b*) and Stietel *et al.* (1996), for 'Poiseuille cracks'.

Finally, we are continuing the extension of our theoretical frame for obtaining equivalent continuum H-M laws and coefficients for more general types of *dual porosity media*, including not only the current case of a fractured porous claystone comprising small statistical cracks as well as large curved fracture surfaces, but also other types of heterogeneous geological media as well, for example, with cavities and holes rather than thin cracks.

The first two authors wish to acknowledge financial support by Andra.

Appendix 1

Equivalent isotropic coefficients from fourth-rank stiffness R_{ijkl}

The equivalent continuum (upscaled) material coefficients obtained in this work are *not* assumed to be orthotropic at voxel scales (see discussion in Section 3.4). However, on large transverse scales of averaging (e.g. annular averaging), we have derived equivalent scalar quantities from the upscaled tensorial coefficients. These scalars are obtained from spherical equivalent tensors, through a procedure we have called '*isotropization*'. This is briefly explained in this Appendix. Let us first review the list of tensorial continuum equivalent coefficients in this paper:

- B_{ij} – *stress–pressure coupling Biot coefficient (second-rank tensor).* In this case, the 'isotropized' value B is obtained by taking the spherical part of B_{ij}, that is: $B = (B_{kk})/3 = \mathrm{Tr}(\underline{\underline{B}})/3$ where $\mathrm{Tr}(\underline{\underline{B}})$ is the trace of tensor $\underline{\underline{B}}$.
- M – *fluid production–pressure coupling (scalar Biot modulus*). This coefficient is by essence a scalar, that is, a zero-order tensor (it does not require 'isotropization').
- R_{ijkl}, C_{ijkl} – *stiffness and compliance coefficients (fourth-rank tensors).* These upscaled coefficients are generally non-isotropic and non-orthotropic tensors, although they do have all the other symmetries of elasticity (this is one of the consequences of the linear superposition method).

We expect the upscaled elastic tensors R_{ijkl} and C_{ijkl} to become isotropic in the case of geometrically isotropic materials. We have verified that this is indeed the case via numerical tests with statistically isotropic and homogeneous fracturing (*not shown here*). In the isotropic case, the classical scalar coefficients of isotropic elasticity (E, ν, μ, etc.) can be directly extracted from the fourth-rank tensors (R_{ijkl} or C_{ijkl}). Our goal is to obtain similar scalar

coefficients for the case of non-isotropic/non-orthotropic upscaled materials.

To simplify the analysis of upscaled tensorial coefficients, we can extract algebraic subsets from the fourth-rank stiffness and compliance tensors (R_{ijkl}, C_{ijkl}), as explained in the text (section 'Inputs, outputs and post-treatment of hydro-mechanical upscaling'). Let us focus in particular on 'shear stiffness' (Pa) or 'shear compliance' (Pa^{-1}) submatrix S_{IJ}, which contains the nine stiffness coefficients $R_{2323}, \ldots, R_{2312}, R_{1313}$ (similarly for compliance). Using Kelvin's well-known 6×6 index notation for R_{ijkl}, this 3×3×3×3 tensor can be expressed as a 6×6 matrix R_{IJ} with indices $I \in \{1, \ldots, 6\}$, $J \in \{1, \ldots, 6\}$, where $I = \{1, 2, 3, \text{and } 4, 5, 6\}$ corresponds to $(i, j) = \{(1, 1), (2, 2), (3, 3) \text{ and } (2, 3), (1, 3), (1, 2)\}$. The (3×3) shear submatrix S_{IJ} (analysed in Table 6) corresponds to the symmetric lower right part of the (6×6) R_{IJ} matrix. Note that the R_{IJ} matrix, with Kelvin's notation, does *not* represent a (6×6) second-rank tensor. For the same reason, S_{IJ} is a matrix rather than a tensor, *a priori*. Nevertheless, S_{IJ} being a symmetric (3×3) matrix which also appears to be positive-definite (or at least positive), it can be diagonalized, and then, it can be represented by an ellipsoid – which reduces to a sphere in the case of isotropic shear behaviour. Finally, a few words about notation: '*S*' stands for 'shear'; the diagonal components of S_{IJ} can be labelled S_{44}, S_{55}, S_{66} with Kelvin's (I, J) notation, but they could be labelled S_{11}, S_{22}, S_{33} if we revert to the standard notation S_{ij} for a 3×3 matrix with $i = \{1, 2, 3\}$ and $j = \{1, 2, 3\}$. Note also that S_{IJ} represents shear stiffness when it is extracted from R_{ijkl} (Pa), and shear compliance when it is extracted from C_{ijkl} (Pa^{-1}).

We now briefly describe how equivalent isotropic coefficients are defined from fourth-rank mechanical tensors, leading to bulk and shear moduli, Young's coefficient (E) and Poisson's ratio (ν):

Step 1. We define a scalar *bulk stiffness modulus* (K) for a non-isotropic/non-orthotropic material, in terms of the fourth-rank stiffness tensor R_{ijkl}, as follows:

$$3K = R_{ppll}/3 = (R_{1111} + R_{2211} + R_{3311} + R_{1122} + \cdots R_{3322} + R_{1133} + \cdots + R_{3333})/3 \quad \text{(A.1)}$$

Step 2. One can define as follows an equivalent tensor of volumetric stiffness (K_{ijmn}):

$$3K_{ijmn} = 3K\delta_{mi}\delta_{nj} = (R_{ppll}/3)\delta_{mi}\delta_{nj} = (R_{ppll}/3)(\delta_{mi}\delta_{nj} + \delta_{mi}\delta_{nj})/2 \quad \text{(A.2)}$$

The last equality is obtained by exploiting the symmetries of elastic mechanics (these symmetries are conserved by our upscaling: they are applicable to macroscale coefficients).

Step 3. We interpret this relation in terms of the known elastic coefficients that characterize an (equivalent) isotropic material. We do this by inserting, in the K_{ijmn} and R_{ijkl} tensors, their known expressions in terms of Lamé moduli (λ, μ) for an isotropic material. This yields:

$$3K_{ijmn} = 3K(\delta_{mi}\delta_{nj} + \delta_{mj}\delta_{ni})/2 = (3\lambda + 2\mu)(\delta_{mi}\delta_{nj} + \delta_{mj}\delta_{ni})/2 \quad \text{(A.3)}$$

where

$$K = (3\lambda + 2\,\mu)/3 \quad \text{(A.4)}$$

This macroscale result is as expected, and it is also consistent with the scalar K that we directly introduced in the first step above ($3K = R_{ppll}/3$).

Step 4. Continuing the previous comparison process with the case of isotropic materials, we introduce the Young modulus, E, and the Poisson ratio, ν, and we keep the shear modulus, μ, to describe the equivalent isotropic material. Thus:

$$3K = (3\gamma + 2\mu);\ E = 3\ (1 - 2\nu);\quad E = 2\mu(1 + \nu) \quad \text{(A.5)}$$

Step 5. Defining for isotropic materials the shear stiffness modulus as $G = 2\mu$ (instead of the more usual $G = \mu$), we extend this notion to a shear stiffness tensor G_{ijmn} for the case of a non-isotropic/non-orthotropic material, again in terms of the fourth-rank stiffness tensor R_{ijkl}:

$$G_{ijmn} = R_{ijmn} - R_{ppmn}\delta_{ij}/3 \quad \text{(A.6a)}$$

Step 6. For isotropic materials, the shear stiffness tensor Gijmn reduces to:

$$G_{ijmn} = 2\mu(\delta_{mi}\delta_{nj} + \delta_{mj}\delta_{ni})/2 \quad \text{(A.6b)}$$

For verification, one can show that the scalar shear stiffness $G = 2\mu$ is indeed obtained upon introducing the isotropic version of the G_{ijmn} tensor (as given just above in equation A.6b) into the general fourth-rank tensor R_{ijkl}, and then assuming isotropy of the fourth-rank R_{ijkl}.

Step 7. Further contractions of the non-isotropic Gijmn of equation (A.6a) can lead to the equivalent isotropic form of equation (A.6b), and this eventually defines the scalar equivalent G or μ.

In summary, when dealing with fully non-orthotropic materials, we can use contracted forms of the fourth-rank stiffness tensor R_{ijkl} to define isotropic scalar equivalents of the classical coefficients of isotropic elasticity (K, E, ν, μ). We proceed similarly for the H-M coupling coefficients: thus, the spherical part of the second-rank Biot tensor B_{ij} yields the scalar B. We call this procedure '*isotropization*' (isotropic equivalents for fourth- and second-rank tensors).

References

Ababou, R., Millard, A., Treille, E., Durin, M. & Plas, F. 1994*a*. Continuum modeling of coupled thermo-hydro-mechanical processes in fractured rock. *In*: Peters, A. *et al.* (eds) *Computational Methods in Water Resources*. Kluwer Academic, Dordrecht, **1**, 651–658.

Ababou, R., Millard, A., Treille, E. & Durin, M. 1994*b*. *Coupled thermo-hydro-mechanical modeling for the near field benchmark test 3 (BMT3) of DECOVALEX phase 2 – progress report*. Rapport DMT/93/488, Commissariat à l'Energie Atomique, Saclay, France, 17 May.

Ababou, R., Cañamón, I. & Poutrel, A. 2011. Macropermeability distribution and anisotropy in a 3D fissured and fractured clay rock: 'excavation damaged zone' around a cylindrical drift in Callovo-Oxfordian argilite (Bure). *In*: *Special issue on 'Clays in Natural and Engineered Barriers for Radioactive Waste Confinement' (4th International Meeting, CLAYS 2010*, Nantes, 29 March to 1st April 2010). *Journal of Physical and Chemistry of the Earth*, **36**, 1932–1948. http://dx.doi.org/10.1016/j.pce.2011.07.032

Ababou, R., Cañamón, I. & Poutrel, A. 2012. 3D Hydro-mechanical homogenization and equivalent continuum properties of a fractured porous claystone around a gallery: application to the damaged and fractured zone at the Meuse/Haute-Marne Underground Research Laboratory. *In*: *Proceedings of the International Conference CLAY 2012: Clays in Natural and Engineered Barriers for Radioactive Waste Confinement*, 22–25 October 2012, Montpellier, France, Poster Session 'Geomechanics/Numerical Modeling': poster Gm/NM/19, extended abstract.

ANDRA 2005*a*. *Dossier Andra 2005 (collective publication)/Rapport Technique ANDRA CRPADS040022 (collectif, 15 déc. 2005)*. Dossier 2005 – Référentiel du Site Meuse/Haute-Marne – Tome 2, **7**, chap. 32.

ANDRA 2005*b*. *Évaluation de la faisabilité du stockage géologique en formation argileuse. Dossier 2005 Argile. Synthèse: évaluation de la faisabilité du stockage géologique en formation argileuse*. ANDRA, December.

Armand, G. & ANDRA 2007. Analyse des perméabilités mesurées autour des ouvrages du LSMHM au niveau − 490 m pour déterminer des lois empiriques utilisables dans des calculs hydromécaniques couplés en milieu continu (Laboratoire de Recherche Souterrain de Meuse/Haute-Marne). Note Technique ANDRA D.NT.ALS.07.0453 A, 24 May.

Bailly, D. 2009. Vers une modélisation aux grandes échelles des écoulements dans les milieux très fissurés de type karst: étude morphologique, hydraulique et changement d'échelle. Doctoral thesis, Institut National Polytechnique de Toulouse, Université de Toulouse, France, 24 June, http://ethesis.inp-toulouse.fr/archive/00000975/

Bailly, D., Ababou, R. & Quintard, M. 2011. Macropermeability K of highly fissured porous media: inertial and percolation effects. *In*: *EGU 2011: General Assembly 2011 of the European Geosciences Union (Session HS8.2.1: Stochastic Groundwater Hydrology)*, Vienna, Austria, 3–8 April 2011, poster and abstract. Geophysical Research Abstracts, **13**, EGU 2011-4718.

Basser, P. J. & Pajevic, S. 2007. Spectral decomposition of a 4th-order covariance tensor: applications to diffusion tensor MRI. *Signal Processing*, **87**, 220–236.

Biot, M. A. 1941. General theory of three-dimensional consolidation. *Journal of Applied Physics*, **12**, 155–164.

Biot, M. A. 1956. General solutions of the equations of elasticity and consolidation for a porous material. *Journal of Applied Mechanics*, **23**, 91–96.

Cañamón, I. 2009. *Coupled Phenomena in 3D Fractured Media Analysis and Modeling of Thermo-Hydro-Mechanical Processes)*. VDM Verlag.

Cañamón, I., Elorza, F. J. & Ababou, R. 2006. 3D fracture networks: optimal identification and reconstruction. *In*: *Proceedings of IAMG'06: International Association of Mathematical Geology, XIth International Congress*, University of Liège, Belgium, 3–8 September.

Cañamón, I., Ababou, R. & Elorza, F. J. 2007. A 3-dimensional homogenized model of coupled thermo-hydro-mechanics for nuclear waste disposal in geologic media. *In*: *Proceedings of ENC 2007 (European Nuclear Conference 2007): 'Nuclear Waste Modeling'*, Brussels, 16–20 September, http://www.euronuclear.org/events/enc/enc2007/home.htm.

Cañamón, I., Ababou, R. & Elorza, F. J. 2009. Numerical modeling and upscaling of a 3D fractured rock with Thermo-Hydro-Mechanical coupling. *In*: Amaziane, B. *et al.* (eds) *Proceedings of MAMERN09, 3rd International Conference on Approximation Methods and Numerical Modelling in Environment and Natural Resources*, Pau, France, 8–11 June, Editorial Universidad de Granada.

Charlez, Ph. A. 1991. *Rock Mechanics, Volume 1, Theoretical Fundamentals*. Editions Technip, Paris.

Cosenza, P., Ghoreychi, M., De Marsily, G., Vasseur, G. & Violette, S. 2002. Theoretical prediction of poroelastic properties of argillaceous rocks from in situ specific storage coefficient. *Water Resources Research*, **38**, 1207, http://dx.doi.org/10.1029/2001WR001201

Coste, F., Bounenni, A. & Chanchole, S. 1999. *Evolution des propriétés hydrauliques et hydromécaniques lors de l'endommagement des argilites de l'Est. Paper at Journées Scientifiques 'Etude de l'Est du Bassin Parisien'*. ANDRA and CNRS, Nancy, France, December.

Coussy, O. 1991. *Mécanique des Milieux Poreux*. Editions Technip, Paris.

Darcy, H. P. G. 1856. *Les Fontaines Publiques de la Ville de Dijon, Exposition et Application des Principes à Suivre et des Formules à Employer dans les Questions de Distribution d'Eau*. Victor Dalmont, Paris, Appendix D.

Mehrabadi, M. M. & Cowin, S. C. 1990. Eigentensors of linear anisotropic elastic-materials. *Quarterly Journal of Mechanics and Applied Mathematics*, **43**, 15–41.

Mourzenko, V. V., Bogdanov, I. I., Thovert, J. F. & Adler, P. M. 2010. Three-dimensional numerical simulation of single-phase transient compressible flows and well-tests in fractured formations. *Mathematics and Computers in Simulation*, **81**, 2270–2281.

Oda, M. 1986. An equivalent continuum model for coupled stress and fluid flow analysis in fractured rock masses. *Water Resources Research*, **22**, 1845–1856.

Oda, M. & Hatsuyama, Y. 1985. Permeability tensor for jointed rock masses. *In*: *Proceedings of International Symposium on Fundamentals of Rock Joints*, Bjorkliden, 15–20 September, 303–312.

Pouya, A. 2007. Ellipsoidal anisotropies in linear elasticity – extension of Saint Venant's work to phenomenological modelling of materials. *International Journal of Damage Mechanics*, **16**, 95–126.

Pouya, A. 2011. Ellipsoidal anisotropy in linear elasticity: approximation models and analytical solutions. *International Journal of Solids and Structures*, **48**, 2245–2254.

Sævik, P. N., Berre, I., Jakobsen, M. & Lien, M. 2013. A 3D computational study of effective medium methods applied to fractured media, *Transport in Porous Media*, **100**, 115–142.

Stietel, A., Millard, A., Treille, E., Vuillod, E., Thoraval, A. & Ababou, R. 1996. Continuum representation of coupled hydro-mechanical processes of fractured media: homogenisation and parameter identification. *In*: Stephansson, O., Jing, L. & Tsang, C-F. (eds) *Coupled Thermo-Hydro-Mech. Proceedings (Decovalex International Project)*. Developments in Geotechnical Engineering. Elsevier, Amsterdam, **79**, 135–164.

Terzaghi, V. K. 1936. The Shearing Resistance of Saturated Soils and the Angle between the Planes of Shear. *In*: *First International Conference on Soil Mechanics*. Harvard University Press, Cambridge, MA, **1**, 54–56.

Vincké, O., Longuemare, P., Boutéca, M. & Deflandre, J. P. 1997. *Etude du comportement poromécanique d'argilites dans les domaines élastiques et post-élastiques. Paper presented at Journées Scientifiques 'Etude de l'Est du Bassin Parisien*. ANDRA and CNRS, Bar-le-Duc, France, October.